Pasztorek et al,. J Regen Med 2021, 10:1

DOI: 10.37532/jrgm.2021.10(1).176

Journal of Regenerative Medicine

Research Article

A SciTechnol Journal

Stress Fiber Formation, Mitochondrial Morphology and Membrane Properties of Human Mesenchymal Stem Cells Cultured in Plastic Adherence or in Spherical Aggregates

Markus Pasztorek[1], Daria Mrazova[2], Eva Rossmanith[1], Sonja Walzer[3], Sabine Rauscher[4], Marion Groeger[4], Viktoria Weber[1,5], Renata Rychtarikova-Stysova[2], Dalibor Stys[2], and Michael B. Fischer*[1,5,6]

Abstract

Relevance: Mesenchymal stem cells (MSCs), when cultivated in adherence to plastic surfaces, develop large bundles of actin filaments with mechanosensitive properties. These stress fibers induce tension forces via focal adhesions bound to the extracellular matrix, thereby influencing elastic properties of the cell membrane relevant for MSC function.

Methods: Actin was quantified in plastic adherent MSCs or in aggregate cultures using flow cytometry and Western blotting. Stress fiber formation, connection to focal adhesions and mitochondrial dynamics were investigated by laser scanning microscopy. Surface morphology and membrane properties of MSCs were performed by atomic force microscopy and migration was measured in a wound closure assay.

Results: Total actin protein remained largely unchanged during cultivation of MSCs from passage (P)1 to P3, but distribution of bold stress fibers changed. Ventral stress fibers, anchored at each end to focal adhesions, increased in fiber length during cultivation, while dorsal stress fibers anchored at one end to focal adhesions, increased in number.

Mitochondrial branching during cultivation from P1 to P3 gave further evidence for deficits in fusion/fission kinetics. Deflection scanning by AFM confirmed these observations by showing intense bundles of stress fibers in P1 and P3 MSCs, while MSC emerging from aggregates showed discrete stress fiber morphology. Force vs indentation profiles of native MSCs with exclusion of nuclear regions showed the highest Young's moduli of 8.5 ± 6.4 kPa in P1, followed by 6.5 ± 6.1 kPa in P3 MSCs and 3.6 ± 3.2 kPa for MSCs of spherical aggregates.

Conclusion: When MSCs are expanded for potential therapeutic use, stress fiber morphology with increased length of ventral stress fibers and higher number of dorsal stress fibers can increase the inner force of MSCs resulting in changes of their physical properties. Mitochondrial branching in passaged MSCs gave further evidence for a decline in cell function.

***Corresponding author:** Michael B. Fischer, Department for Health Science and Biomedicine, Danube University Krems, Krems, Austria, Tel: + 00436649166807; E-mail: michael.fischer@donau-uni.ac.at

Received: January 27, 2021 **Accepted:** February 26, 2021 **Published:** March 05, 2021

Keywords

Mesenchymal Stem Cells; Spherical Aggregate Cultures; F-actin, Focal Adhesion; Young's Modulus; Stress Fibers

Introduction

Mesenchymal stem cells (MSCs) isolated from bone marrow, adipose tissue, or from the placenta are potent candidates for cell-based therapies in diverse clinical applications in order to support tissue regeneration or mediate immune modulation [1,2]. Advancement of tissue engineering, however, relies on the ability of MSCs to be directed towards a specific cell phenotype and their capability to integrate into the damaged target tissues [1]. Naturally occurring or artificially applied external forces affect self-maintenance, proliferation, and differentiation of MSCs by mechanisms dependent on the integration of mechanically induced signaling cascades [3,4]. Internal forces achieved by MSC-matrix interaction, in addition, can generate contractile forces to sense mechanical properties of the biomaterial comprising topography and rigidity of the substrate. [4-8].For MSCs and the lineage specific cells they generate, adhesion and retention in the local environment of tissue and organs are processes predicated on the cells' mechanobiological capability [9].

When MSCs are grown ex vivo in adherence to plastic surfaces as recommended by the International Society for Cell Therapy (ISCT) or bound to extracellular matrix (ECM) components attached to plastic or glass surfaces, the most prominent cytoskeletal structures appearing are stress fibers (SF) [10-12]. SFs show mechanosensitive properties and comprise large bundles of actin filaments (f-actin) and associated proteins, typically located at the ventral surface of the cell anchored at both ends to focal adhesions (FA) [12-17]. These ventral SFs are frequently several micrometers long extending most of the length of the cell [3,12]. Dorsal SFs that appear radial and anchor at just one end to a FA are usually much shorter and form just behind the leading edge of the cell in motion [3,12]. In moving and spreading cells, potential contractile bundles of actin filaments termed 'transverse arcs' develop typically at the basis of lamellipodia [3,12]. The tension forces generated by SFs are transmitted to the extracellular matrix via integrin-containing FAs [12-14]. These multi-protein subcellular structures composed of talin, alpha- actinin, filamin, vinculin, focal adhesion kinase (FAK) and tensin (integrin-adaptor protein-cytoskeleton) are in a constant flux in the cytoplasm with proteins associating and dissociating [12-17]. Due to a reciprocal dynamic of the force balance, cell-generated forces can be transmitted across integrin-containing FAs to the MSC surrounding ECM network controlling cell shape, regulate the balance between cell growth, differentiation and death [7,9,12,18]. Furthermore, cytoskeletal tension is also involved in ECM remodeling and initiation of an autologous ECM environment in spherical aggregate MSC cultures [19]. Downregulation of pluripotent genes such as Oct4, Sox2 and Nanog with loss of self-renewal are several drawbacks of MSCs cultured in the absence of ECM remodeling signals, while spherical cultures preserve their pluripotent status [20]. These results showed a direct MSC-ECM reciprocity involving a chemo-mechanical coupling at the cell-material interface[3,12,16,21-26].

Here, we investigate (1) the effect of cultivation on the development of SFs in placenta derived human MSCs; (2) how SFs are connected to the supportive surface they are attached to by FAs, (3) whether mitochondrial dynamics are affected, (4) how cultivation can influence force deformation of the membrane determined by atomic force microscopy (AFM) and (5) how cultivation up to P3 can influence migratory capability of MSCs in a wound closure assay. Replies to these issues would advance our understanding of the mechanobiological behavior of MSC during cultivation, as well as would provide basic information on MSCs' migratory capability to propel tissue repair.

Materials and Methods

Processing of placenta tissue, 2D and 3D MSC cultures and flow cytometry analysis

The amnion membrane was dissected into 3 x 3 cm squares, washed in physiological saline and digested with dispase (2.5 CU/ml, Becton Dickinson, Franklin Lakes, NJ) [27]. Thereafter, tissues were incubated with a mix of collagenase A (1 mg/ml) and DNase I (0.01 mg/ml, both Roche, Basel, Switzerland) and supernatants were strained using a 100 µm strainer to separate cells. Single cells were adhered to plastic surfaces to propagate MSCs in 2D within MSCGMTM- medium (Lonza Group Ltd., Basel, Switzerland) supplemented with 100 U/ml penicillin, 100 µg/ml streptomycin and 250 ng/ml amphotericin B (all from Gibco, Thermo Fisher Scientific, Waltham, MA) at 37 °C in 5 % CO_2 humidified environment (Stericycle, Thermo Fisher Scientific, Waltham, MA). The medium was changed every three to four days, and MSCs were passaged at 80 % confluence. The living MSCs (Live/Dead Cell Assay, Invitrogen, Thermo Fisher Scientific, Waltham, MA) of P1 and P3 were characterized with ecto-5'-nucleotidase (CD73), Thy-1 a glycophosphatidylinositol (GPI) anchored conserved cell surface protein (CD90) and for endoglin a component of the receptor complex of TGF-β (CD105) mAb (1 µg/ml, all from eBioscience, Thermo Fisher Scientific, Waltham, MA) using a Gallios 10/3 flow cytometer (Beckman Coulter GmbH, Krefeld, Germany). Actin was quantified using AlexaFluor (AF) 488 labeled phalloidin (0.1 U/ml, Molecular Probes, Thermo Fisher Scientific, Waltham, MA) and size measurements were performed with silica beads (1.5 µm, Beckman Coulter GmbH, Krefeld, Germany; 30 and 65 µm, Kisker Biotech, Steinfurt, Germany). For 3D MSC spherical aggregates, P0 MSCs in a concentration of 5,000 cells per aggregate were cultivated in hanging drops at 37°C in 5 % CO_2 air humidified environment for two days. Three-lineage differentiation of MSCs into chondrogenic, osteogenic, and adipogenic lineage (Figure 1) was performed using standard protocols. [28].

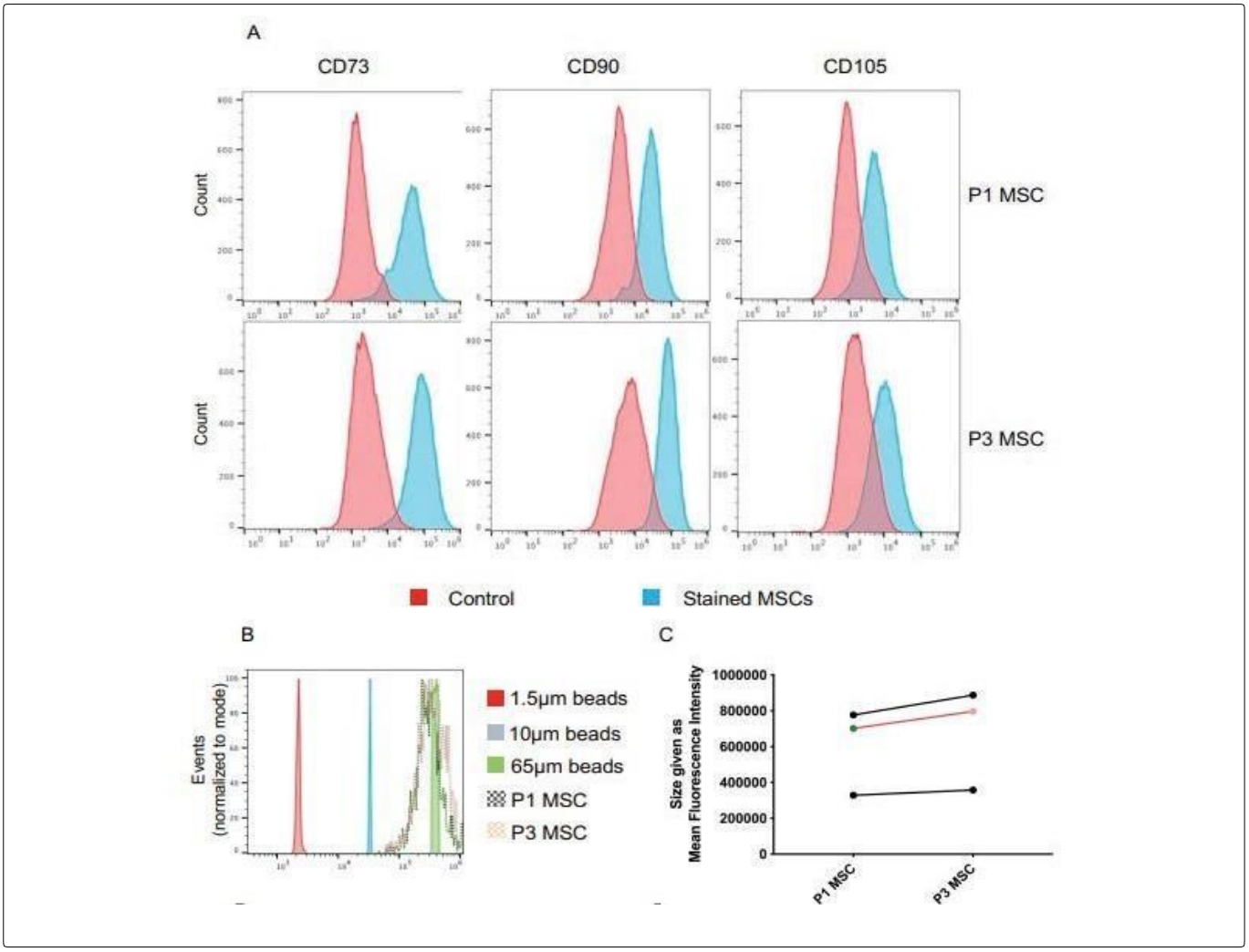

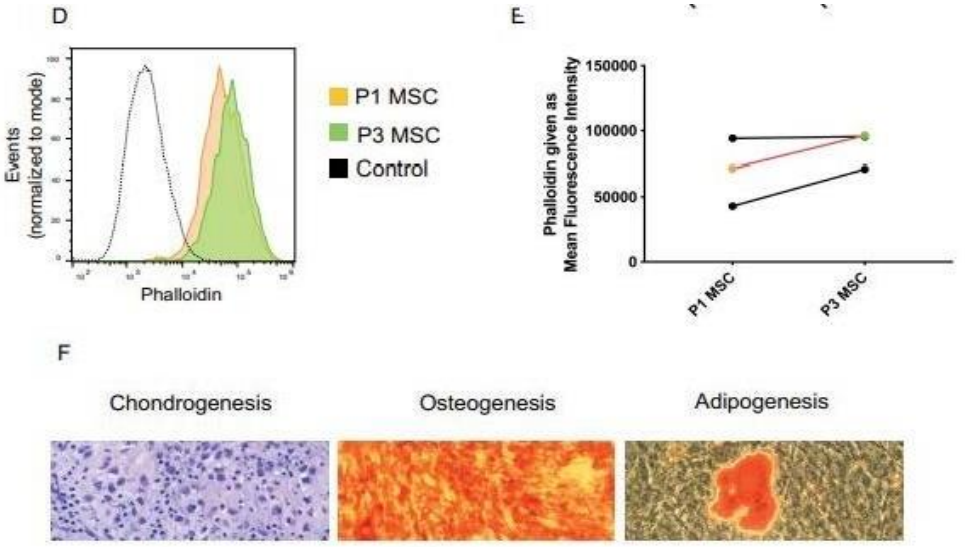

Figure 1: (A) Flow cytometric measurement of passage 1 (P1) and passage 3 (P3) living MSCs stained with anti-CD73, anti-CD90 and anti-CD105. (B) Size measurements of P1 and P3 MSCs by flow cytometry using 1.5 µm, 10 µm and 65 µm silica beads. (C) Dot plot of the mean fluorescence intensity of three batches of 2,000 cells per batch (n=3). (D) Actin measurements with phalloidin of living CD90+ P1 and P3 MSCs determined by flow cytometry. (E) Dot plot of the mean fluorescence intensity of three batches of 5,000 cells per batch (n=3). (F) Left: Alcian blue staining indicates chondrogenic differentiation. Middle Alizarin red staining indicates osteogenic differentiation. Right: Oil red staining indicates adipogenic differentiation.

High resolution imaging by scanning electron microscopy

Scanning electron micrographs were obtained using a FlexSEM 1000 (Hitachi Ltd. Corp., Tokio, Japan) with SEM MAP camera navigation to investigate the single adhered MSCs in either P1 or P3 and the spherical MSC aggregates. For this purpose, the spherical MSC aggregates or a suspension of 1 x 106 MSCs/ml were incubated in 24 well plates (Nunc, Thermo Fisher Scientific, Waltham, MA) on NuncTMThermanoxTM coverslips (Nunc, Thermo Fisher Scientific, Waltham, MA). After 16 hours, the coverslips were fixed with 2.5 % glutaraldehyde (Sigma-Aldrich, St. Louis, MO) and dehydrated by stepwise alcohol extraction from 50 % - 100 %. Dried coverslips were mounted on EM-Tec CT12 conductive double side adhesive carbon tabs (Micro to Nano V.O.F., Haarlem, Netherlands) with a diameter of 12 mm and surface sputtered with gold using a QuorumTech Q150T ES (Quorum Tech Ltd., Laughton, UK) for betterresolution.

Western blotting to semi-quantify cellular actin

P1 and P3 MSCs were sorted using an Aria Fusion CellSorting device (Becton Dickinson, Franklin Lakes, NJ) for a total of 300,000 MSCs. Cells were then lysed with 1 % protease phosphatase inhibitor in RIPA extraction buffer and (both from Invitrogen), total protein was measured using a protein assay (Biorad, Hercules, CA). Aliquots of 7 µg protein were loaded on precast 4-12 % polyacrylamide Bis-Tris gels (NuPAGE Novex, Invitrogen) in a NuPage MOPS-buffer and SDS-PAGE western blotting was performed using a XCell SureLock TM Mini-Cell and a PowerEase 500 W power supply (Invitrogen). Separated molecules were transferred on nitrocellulose membranes witha 0.2 µmpore sizeby an XCell IIblotTMmodule. Membraneswere subsequently blocked with non-fat dry milk (Biorad, Hercules, CA). A primary anti-actin antibody (0.2 mg/ml, Abcam, Cambridge, UK) was detected with a HRP conjugate and a Clarity Max Western ECL blotting substrate (Biorad, Hercules, CA) and the chemiluminescent signal was recorded with a Chemi-Doc documentation system (Biorad, Hercules, CA) for semi-quantification. For internal control, purified actin protein (Cytoskeleton Inc., Denver CO) was used at a total concentration of 400 to 700 mg.

Confocal laser scanning microscopy (LSM)

The P1 and P3 MSCs as well as MSC emerged from spherical aggregates were treated with a fixation and permeabilization reagent (eBioscience, Thermo Fisher Scientific, Waltham, MA) and incubated either with vinculin (2 µg mouse mAb/ml, clone 7F9, Santa Cruz Biotechnology, Dallas, TX), with paxillin (2 µg mouse mAb/ml, clone B2 Santa Cruz Biotech) to reveal FAs, with vimentin (3.6 µg mouse mAb/ml, clone 1/9, Dako Products, Agilent, Santa Clara, CA) to label the intermediate filaments, or with the MitoTracker Red CMX Ros (Molecular Probes, Thermo Fisher Scientific, Waltham, MA) to reveal mitochondria, followed by incubation with AF-488 or AF-594 goat anti-mouse polyclonal Fab fragment Ab as second antibody (3 µg/ml, Jackson Laboratories, Bar Harbor, MN). The MSCs were counterstained with AF-488 or AF-594 phalloidin (0.1 U/ml, Molecular Probes, Thermo Fisher Scientific, Waltham, MA) to label f-actin and finally nuclei were stained with DAPI (Sigma-Aldrich, St. Louis, MO). To avoid bleaching the slides were mounted with Fluoromount-Gtm (Southern Biotechnology, Thermo Fisher Scientific, Waltham, MA). Serial dilutions of each primary and secondary antibody were tested to minimize non-specific adsorption, assure separation of the fluorescent signals, and optimize fluorophore concentration to preclude self-quenching. Adequate isotype specific controls were included, and images were generated with the same acquisition mode using an alpha-Plan-Apochromat 63x objective and a Leica TCS SP8 confocal microscope (Leica Microsystem GmbH, Wetzlar, Germany).

Tissue Gnostics technology for a context-based actin evaluation

The single MSCs stained with Alexa Fluor® (AF)-635 phalloidin (Invitrogen, Thermo Fisher Scientific, Waltham, MA) and vinculin (Santa Cruz Biotechnology) were scanned using a LSM and analyzed

for the presence of dorsal or ventral SFs as well as transverse arcs using an analysis software StrataQuest (TissueGnostics, Vienna, Austria). Context-based quantitative analysis of fluorescence images was performed on an automatic interface segregating dorsal SFs, from ventral SFs and transverse arcs.

Atomic force microscopy (AFM) scans elasticity measurements and calculation of the inflection point

AFM measurements were carried out using a Nano Wizard® 3 Bioscience AFM (JPK Instruments, Berlin, Germany) with a maximum horizontal scanning range of 100 x 100 µm2 and a vertical range of 15 µm. Triangular silicon nitride cantilevers (spring constant 0.01 N/m, resonance frequency of 7 kHz; supplied by MLCT, Bruker Corporation Camarillo, CA) were used to scan unfixed cells that were imaged with 1024 × 1024 px2 at line rates 0.89 Hz. Topographic images of individual MSCs were visualized in both deflection and height mode. For elasticity measurements, colloidal CP-PNPL-SiO probes (spring constant 0.08 N/m, resonance frequency 17 kHz, sphere diameter 6.62 µm, length 200 µm; supplied by NanoAndMore GmbH, Wetzlar, Germany) were used. Force vs. indentation profiles were recorded at 0.7 Hz. Averages of trace and retrace were used. For finding possible difference in behavior of the Young moduli over the whole range of the cell indentation, we used relation $d = \sqrt[3]{\frac{9(1-\nu^2)^2 F^2}{16E^2 R}}$ that arises from the Hertz model with the Sneddon modification for the elastic indentation of a flat and soft sample by a stiff cone or sphere [29-31]. In this relation, d is the indention depth due to the loading force F, E is the Young modulus, υ is the Poisson ratio for the sample (providing cells are linearly elastic, isotropic, and incompressible at small strains, υ = 0.5), R is the radius of the sample/cell. The loading force was evaluated prior to the force measurement as F(N)=cantilever sensitivity (m/V)×deflection (V)×spring constant(N/m),

Where the sensitivity is defined as the conversion factor from measured voltage to the deflection of the cantilever in nm. The calibration of the sensitivity was performed on a bare glass coverslip each time when the cantilever was remounted.

The deformation curves *F=f(d)* were analyzed with the JPK SPM data processing software (JPK Instruments, Berlin, Germany). Firstly, offset and/or tilt were removed from the baseline in order to find the contact point. Then, the cantilever bending was subtracted from the piezo movement to yield the indentation; the relation *F=f(d)* was plotted in a linear form in order to obtain the Young modulus as a slope of the line.

Light microscopy and image processing

The cell was scanned under an optical transmission microscope-nanoscope (Institute of Complex Systems, Nové Hrady, CZ) – equipped by a 12-bit color digital camera with a Kodak KAI-16000 chip of 4872 × 3248 resolution (offset 0, gain 1, exposure 94.4 ms) recording a primary raw signal. A Nikon objective (LWD 20 x/0.4, inf/1.2, WD 3.1) which gave an image pixel of 64 × 64 nm^2 was used. The sample was illuminated by two Luminus 360 LEDs charged by the current of 5000 mA. The final z-stack contained 150 images.

The detailed procedure of image processing using a Matlab software is described in [32,33]. The method is based on the assumptions that the image is multifractal and the intensity of the out-of-focus image of the object remains constant, whereas the intensity of in-focus image change significantly through the z-step. The stem cell was segmented from the background using an algorithm, which at each z-level subtracts blurred and relevant unblurred image to create a cumulative binary mask through the whole z-stack [32]. From the whole series, the in-focus image of the cell was selected as that which has the minimal value of the point divergence gain entropy in the green channel at α = 4[33].

MSC migration assay

For the migration assay, P1 and P3 MSCs (30,000 cells/well) were grown in 6 well plates with 2 well biocompatible silicone inserts with a defined 500µm cell-free gap according to the manufacturer's instructions and the analysis was performed according to a previous publication using FIJI, an open source image processing package based on ImageJ

Statistics

Data were expressed as mean ± standard deviation unless otherwise stated. Paired t-test or Wilcoxon test were performed for paired analysis like described in the figure legend. Statistical analysis was performed by the GraphPad Prism software8.

Results

Stress fiber formation in MSCs cultured in adherence to plastic surfaces

Amnion derived MSCs from P1 and P3 cultivated in plastic adherence in MSCGMTM- medium were positive for MSC specific markers CD73, CD90 and CD105, and showed a size of approximately 30-60 µm in diameter (Figure 1 A-C) when compared to silica beads. SF formation, as determined by staining the f-actin cytoskeleton with labeled phalloidin, showed no difference between P1 and P3 cultured MSCs when determined by flow cytometry (Figure 1 D, E, F). When SF formation was further investigated by quantifying the amount of actin by western blotting, the relative actin protein expression showed no difference when normalized to 1 µg total protein obtained from 300,000 sorted P1 or P3 MSCs (Figure 2 A, B). The amount of total protein applied in western blot analysis was 7 µg per lane and using this concentration the amount of actin found in P1 and P3 MSCs corresponded to the internal actin standard ranging from 400 to 700 ng (Figure 2A). For complementation we included a set of phase contrast images to show no morphological difference between the three batches of sorted MSCs (Figure 2 C) although their amount of actin varied.

When SF formation was investigated in P1 and P3 MSCs in a context-based way by confocal laser scanning microscopy, enabling the segregation of SFs into dorsal and ventral as well as transverse arcs (Figure 2 D), we found an increase in number of the dorsal SFs anchored only at one end to FAs in P3 MSCs (Figure 2 E). The remaining sides of the dorsal FAs were found to be attached to the cytoskeleton or the nucleus of the cell. The ventral SFs, in contrast, that span solid f-actin filament bundles from one FA to another tended to increase in length but their number remained constant (Figure 2 F) The transverse arcs, in contrast, showed no response to cultivation (Figure 2 E, F).

Stress fiber formation in MSCs cultured in 3D spherical aggregates

SF formation was investigated in MSCs previously cultivated in hanging-drop cultures to form 3D spherical aggregates (Figure 3 A), a culture technology avoiding plastic adherence and favours an interaction of MSCs with the autologous ECM within the aggregate.

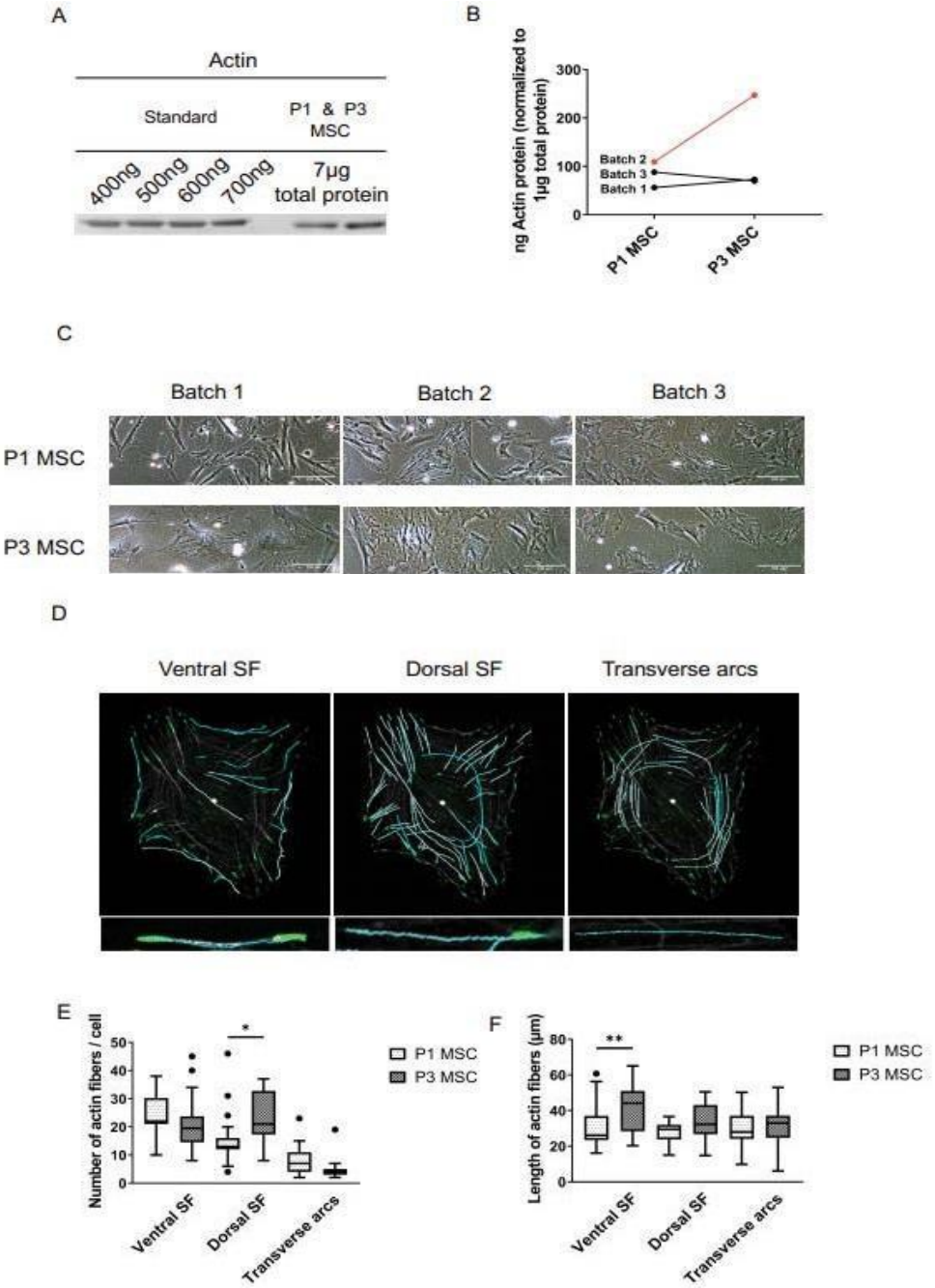

Figure 2: (A) Semi-quantitative western blotting performed with actin protein standard ranging from 400 – 700 ng and actin expression by P1 and P3 MSCs using 7 µg total protein per lane isolated from 300,000 sorted cells. One representative experiment is shown. (B) Relative actin expression in ng actin per g total protein from P1 and P3 MSCs, as determined by western blotting (n=3). (C) Bright-field morphological images are given of the 3 representative batches of cultured P1 and P3 MSCs used in the western botting experiments. (D) Images of ventral, dorsal SFs and transverse arcs in one representative experiment of adhered P1 MSC. (E) Number of ventral and dorsal SFs as well as transverse arcs in adhered P1 and P3 MSCs (n = 20). (F) Length of ventral and dorsal SFs as well as transverse arcs in adhered P1 and P3 MSCs (n = 20), Paired t-test, *$p < 0.05$, **$p < 0.01$.

For this purpose, the single intact 3D spherical MSC aggregates were placed onto plastic surfaces and cultivated for 16 hours under the same conditions as P1/P3 adhered MSCs. During this time MSCs emerged from the aggregates and set up a ring of single adhered MSCs surrounding the spherical aggregate that could be scanned by LSM. These emerging MSCs formed thin and less prominent f-actin filaments as compared with P1 and P3 MSCs grown entirely in adherence to plastic surfaces (Figure 3 B-E) but this technology could only analyze MSCs that emerged out of the aggregates.

Specific components of the FA complex such as paxillin, an FA-associated phosphotyrosine-containing adaptor protein, and vinculin that binds via its amino-terminus to talin, which, in turn, binds to beta-integrins were investigated showing that paxillin and vinculin were found to be intensely expressed in the P1 and P3 MSC as well as

in MSC that emerged from spherical aggregates (Figure 3 B, C) as a result to plastic adherence.

Mitochondrial dynamics in P1 and P3 cultured MSCs

Mitochondrial function in MSCs is linked to morphology. The MSCs are shaped by ongoing events of fusion (merging two organelles into one) and fission (division of a single organelle into two) of inner and outer membranes. We found a higher accumulation of complex mitochondrial networks in P3 MSCs, while in P1 and the mitochondrial distribution in the cytoplasm was more homogeneous distributed (Figure 3 D, F) and complex mitochondrial networks were rare (Figure 3 F). MSCs emerging from spherical aggregates showed also a homogeneous distribution of mitochondria (Figure 3 D) with few networks (data not shown). Vimentin, a type II intermediate filament supporting and anchoring the positions of mitochondria in the cytoplasm, was found to be extensively expressed in adherent P1 and P3 MSCs as well as in adherent MSC emerging from aggregates, indicating that the differences seen in mitochondrial morphology was not due to vimentin (Figure 3 E).

AFM topographic imaging of SF formation in MSC cultivated in 2D and 3D

AFM topographic imaging was performed in deflection and landscape mode to identify cytoskeletal structures in the 2D cultured MSCs on a nanometer scale. The AFM images (Figure 4 A-C) showed

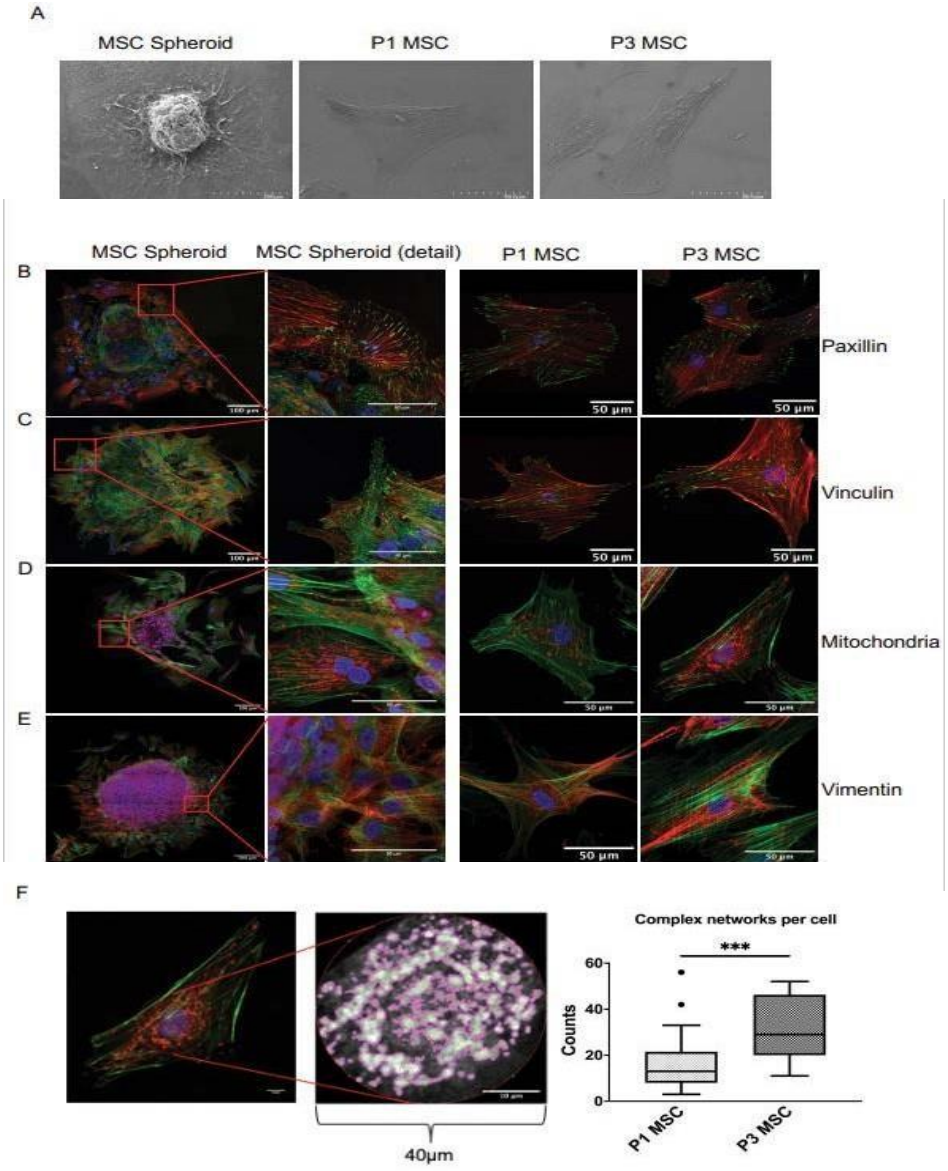

Figure 3: (A) Images of MSC spheroids as well as single adhered P1 and P3 MSCs generated by scanning electron microscopy. (B, C) Images of MSC spheroids in an overview (left) and at higher magnification (middle left) as well as P1 (middle right) and P3 MSCs (right) in high resolution with the specific FA proteins paxillin and vinculin shown in green, SF (f-actin) staining in red and nuclei labeled with DAPI in blue. (D) Mitochondria were stained with MitoTracker in red, SFs in green and nuclei in blue. (E) Alternatively, type-3 intermediate filaments are given by staining vimentin in red, SFs in green and nuclei in blue. The entire MSC spheroid is a maximal intensity projection of a stitched z-stack 3-channel overlay. Magnification for MSC spheroid and the individual MSCs was 63 x. (F) Left & Middle: Confocal image and the corresponding Mitochondrial Network Analysis (MiNA) of the perinuclear region. Right: Numbers of complex mitochondrial networks (>2 branches) per cell (n=30), Wilcoxon test, ***p < 0.001.

doi: 10.37532/jrgm.2021.10(1).176

a flat- and spread-out morphology with crisscross orientated bold sub-membrane SFs with no difference for P1 and P3 cultivation. Interestingly, the best observed SFs in the adhered MSCs were the ventral SFs that span from one cell side to the other. The adhered MSCs originated from a spheroid (ca 50 µm high), in contrast, had a smooth surface with a low amount of sub-membranous SFs (Figure 4 A). Bright field photon transmission microscopy was applied to highlight SFs in single MSCs adhered to plastic surface (Figure 4 D). The life-cell imaging omits the use of dyes and fixation, the intense SF formation visualized by AFM could be confirmed for adhered MSCs.

Young elasticity moduli calculated from P1 and P3 cultured MSCs

We further investigated whether the massive presence of the SFs in adherent MSCs affects their mechanical properties. We measured force-deformation curves of living MSCs' in aqueous media dependent on either P1 or P3. When surface areas were measured without nuclear regions, we found Young's moduli of 8.5 ± 6.4 kPa in P1, followed by 6.5 ± 6.1 kPa in P3 MSCs and 3.6 ± 3.2 kPa in MSCs emerging from aggregates (Figure 4 E). Cultivation condition, however, had

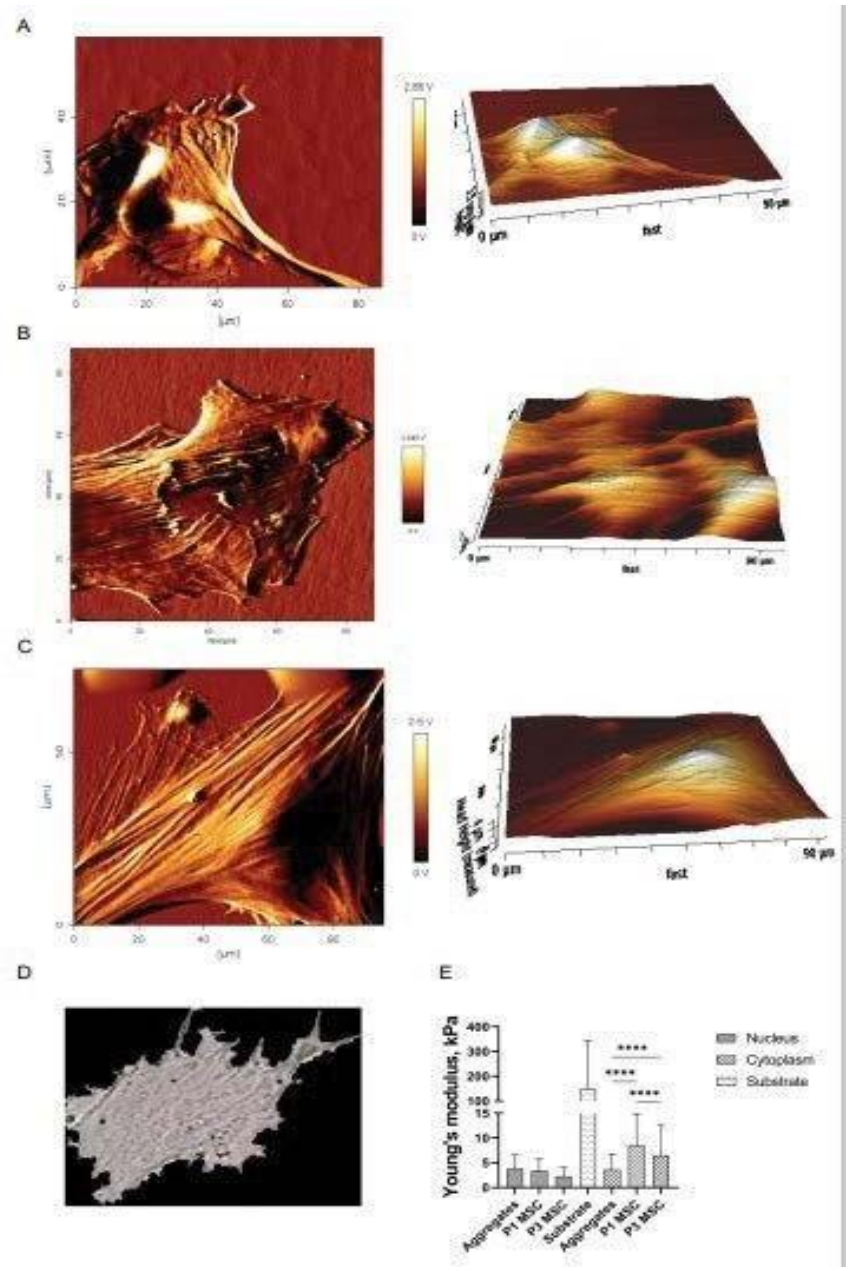

Figure 4: Topographic images of subsurface cytoskeletal structures determined in the nanometer scale range visualized in deflection mode (left) and landscape model (right) by atomic force microscopy. (A) One representative image of a single adhered MSC emanated from the spherical aggregate, (B) a single adhered P1 and (C) P3 MSC. (D) Super-resolved 3- D imaging of MSCs by bright-field photon transmission micrography. (E) Comparison of surface elasticity measurements given by the Young's moduli in MSC spheroids as well as P1 and P3 MSCs with specific segregation between cytoplasmic and nuclear measurements. Substrates moduli of the plastic surface are given as internal control (n=3).

no impact on the nuclear deformability as P1 and P3 MSCs as well as MSCs emerging from aggregates showed no differences in their indentation profiles. The plastic control measurement of culture dish surfaces gave values of (147.9 ± 195.3) kPa.

When the force-vs-indentation profiles were further investigated, results showed that the Young's modulus was not constant over the whole range of indentation (Figure 5 A- C). Two linear slopes could be revealed when the power 2/3 on both sides of the equation was used so that the dependence of the deformation on the force became linear. [34] Examination of force curves revealed an inflection point delineated at the point where the first linear slope (E1) and the second linear slope (E2) touched [34,35]. We found that the slopeofdeflection, according to the applied force, rose gently from contact point (CP) to inflection point (IP) in adherent MSCs emerged from spheroids (ascent: 0.41 ± 0.04) (Figure 5 A-D), indicating that the colloidal AFM tip indented a soft and elastic cell membrane. In P1 MSCs the slope of approach curves calculated was much steeper (ascent: 0.66 ± 0.08) indicating that the colloidal AFM tip indented a stiff but elastic cell membrane (Figure 5 B-D). The slope of approach curves in P3 MSCs was found to be the flattest (ascent: 0.41 ± 0.12), indicating a soft cell membrane (Figure 5 C-D). When the AFM tip moved down passing the inflection point, we found a rise of deflection indicating that the AFM tip touched sub-membrane SFs and organelles (Figure 5 A-C). The interpretation of the curves (E2) gave evidence for high resistance in adherent P1 MSCs (further ascent: 0.97 ± 0.17) (Figure 5 B-E) and low resistance in both adherent P3 MSCs (further ascent: 0.62 ± 0.16) (Figure 5 C right, E) and adherent MSCs emanating from aggregates (further ascent: 0.56 ± 0.01) (Figure 5 A-E).

An additional parameter of elasticity measurements in vital cells is the retraction curve. Under ideal conditions the inner force of the cell drives the AFM tip actively back to the initial contact point. Here we can show that only the MSCs emerging from spherical aggregates had enough driving force to push the AFM tip back to the starting point without any deviation in the retraction curve fit (Figure 5 A). Adherent P1 MSCs showed only a modest effect of differences in the curve fit (Figure 5 B), while adherent P3 MSCs, in contrast, showed the greatest difference between approach and retraction curve (Figure 5 C) most likely due to the negative effect of three rounds of cultivation.

Migratory capability of P1 and P3 MSCs

When the migratory capability of P1 vs P3 MSCs was investigated in a commercially available wound healing assay, where a 500 µm cell-free gap was introduced with a biocompatible silicone insert and closure was investigated after 3, 6, 12 and 24 hours, we found

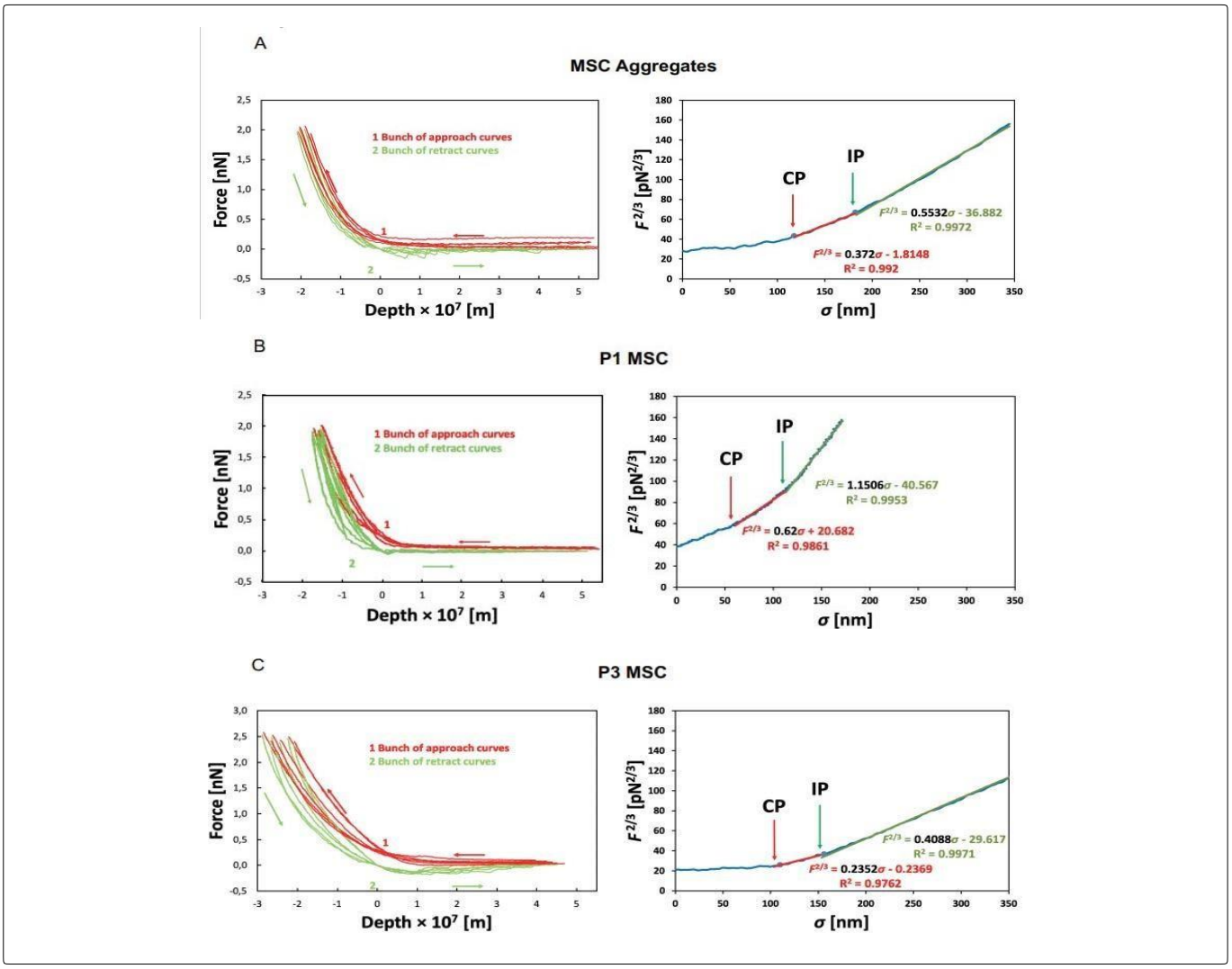

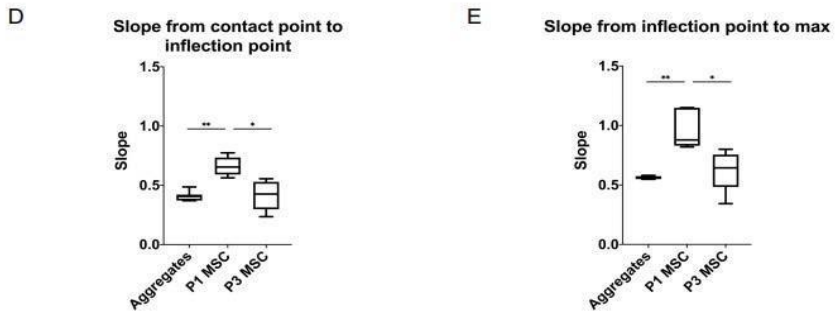

Figure 5: (A-C left) Six representative indentation- (red) and retraction curves (green) of (A left) MSC emerging from spheroids as well as (B left) P1 and (C left) P3 MSCs as determined 30 by atomic force microscopy. (A-C right) Inflection point measurements of (A right) MSC spheroids as well as (B right) P1 and (C right) P3 MSCs to investigate membrane- (E1) and sub-membrane indentation (E2) behavior. (A-C right) A representative curve of contact point (CP) and inflection point (IP) out of the six indentation curves of (A right) MSC emerging from spheroids as well as (B right) P1 and (C right) P3 MSCs as determined by atomic force microscopy. (D) The ascent from contact point to inflection point is given with F2/3 (pN2/3) in red as well as (E) the further ascent from inflection point to the maximum of indentation is given with F2/3 (pN2/3) in green (Aggregates n = 7, P1 MSC n = 5, P3 MSC n = 9), Paired ttest, *p < 0.05, **p < 0.01.

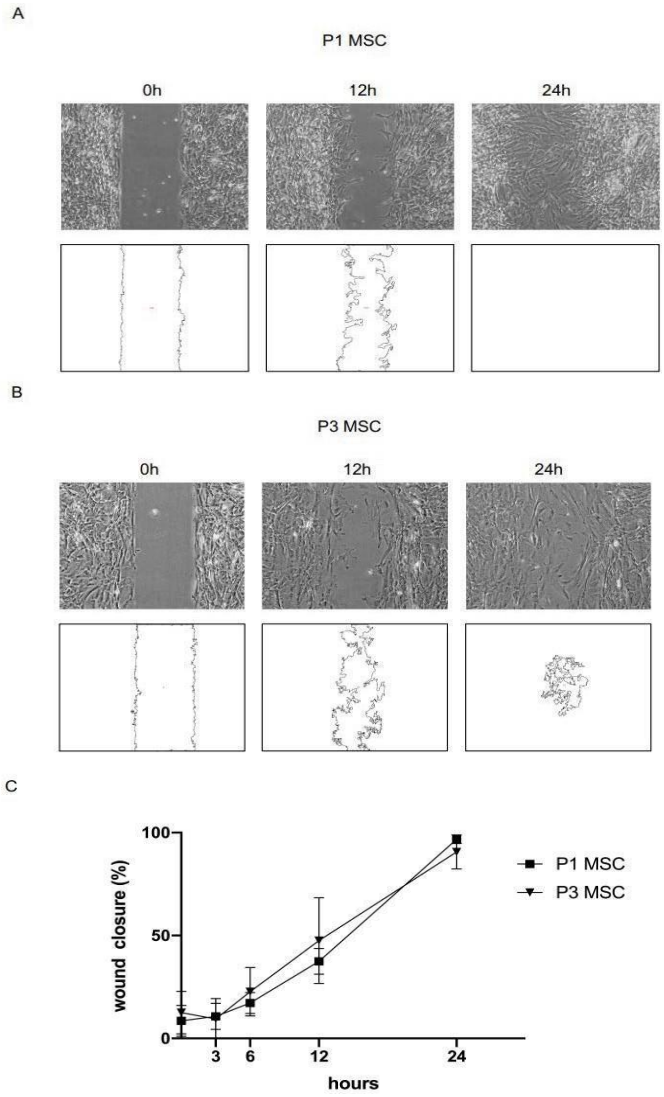

Figure 6: (A) Top: Phase contrast images from P1 MSCs at time point 0h, 12h and 24h, magnification was 4x. Bottom: Image analysis with FIJI (B) Top: Phase contrast images from P3 MSCs at time point 0h, 12h and 24h, magnification was 4x. Bottom: Image analysis with FIJI (C) Comparison of the closure time course of adherent P1 & P3 MSCs (n=5).

comparable closure given in % (of note, 100 % is full closure) of cell-free gap over time (Figure 6 A-C) when analyzed by FIJI, an open-source image processing package based on ImageJ.

Discussion

When MSCs are expanded for a potential therapeutic use, they need to be thoroughly investigated for their potential to assemble SFs. The SFs are of particular importance since they can induce internal force thereby changing cell membrane- and sub-membrane properties [1,10-12]. Although the MSCs' capability to attach, spread, and develops on artificial substrates is a well-defined, physical property according to their structural transformation during the process of cultivation remain less well addressed. We used MSCs isolated from amnion of the placenta to investigate actin formation, the organization of f-actin bundles into SFs and the anchorage of these SFs to FAs upon cultivation on plastic surface. No difference in total actin was found in adhered MSCs during cultivation from P1 to P3 when flow cytometry or western blotting were used. More precisely, both P1 and P3 MSCs showed approximately 400 to 500 ng actin in 7 µg total protein obtained from 300,000 sorted MSCs, normalized to an internal actin standard determined by western blotting. When P1 and P3 MSCs adhered to plastic surfaces were further investigated by LSM, P1 MSCs showed long SFs running in parallel according to the orientation of the MSCs with the occurrence of ventral SFs anchored to FAs on both ends of the actin filaments and dorsal SFs with a radial orientation and only one end attached to FAs. Transverse arcs, in contrast, which are not directly anchored to FAs, occurred less frequently in adhered P1 MSCs and did not change during cultivation. Adhered P3 MSCs showed robust thick crisscross pattern of SFs with few delicate parallel actin filaments as compared with P1 MSCs. Dorsal SFs with only one anchorage to FAs increased during cultivation to P3. The length of the individual ventral SFs, in addition, increased during cultivation, although the number of ventral SFs remained constant. The SFs in cultured MSCs consist of prominent bundles of actin filaments associated with myosin II, alpha-actinin and several actin-binding proteins that can change the helical twist of F-actin in a highly dynamic way [2-9]. The SFs depend on a fine-tuned orchestration of RhoA and their downstream elements that regulates SF assembly involving ROCK that regulates myosin light chain phosphorylation, LIM kinase and RhoA-activated formin (mDia1) as well as molecules stabilizing the actin filaments by inhibiting severing activity of cofilin [12-16]. The MSCs emerging from aggregates, in contrast, did not form any prominent SFs under plastic adherence. These results indicate that adhered MSCs originating from aggregates can set up SFs and induce internal force but not comparable to MSCs grown entirely in adherence. Internal forces are transferred to the outside by FAs that form a complex of vinculin, paxillin, talin, guanine nucleotide exchange factor (GEF)-H1 (fyn-dependent) and FAK to bind both integrins and actin [13-16]. We can show that a robust FA formation occurred with strong expression of vinculin and paxillin in any adhered MSCs of P1, P3 as well as MSCs emerging from aggregates. Inside 3D spherical aggregates, MSCs did not develop FAs although autologous ECM was expressed [36].

The MSCs' mitochondrial morphology, that changes rapidly in response to external stress or metabolic cues, is dependent on signs of unopposed fusion were observed in P3 MSCs. This fusion resulted in a hyperfused networks that serves to counteract metabolic insults, preserve cellular integrity, and protect against autophagy [24]. The evident result was a accumulation of mitochondria of rods and branches and intermediate filaments as part of the cytoskeleton directly followed mitochondrial morphology. Subcellular localization and function was rigorously expressed in the MSCs that were entirely cultivated in adherence to plastic surface, in comparison to the MSCs that emerged from spheroids. It has been previously shown that the binding of mitochondria to vimentin intermediate filaments is tightly regulated by GTPase Rac1. This affects cell physiology, as the timely delivery and distributions of organelles and mitochondria in the cytoplasm is crucial in particular for a fine-tuned fusion and fission process of mitochondria. Here we can show that the differences in mitochondrial morphology in P1 and P3 MSCs as well as MSCs emerging from spherical aggregates was not due to alterations in vimentin expression as vimentin was highly expressed in all three culture conditions.

Another important issue in cell therapy is the impact of mechanical properties. The MSCs experience mechanical stretch, compression or tension forces throughout their lifetime in tissue and organs. The constant exposure of MSCs to external force is critical to maintain their functional balance. [34,35,37] Isometric tension mediated by ventral SFs led to disassembly of preexisting SFs in adhered MSCs, while synchronous reassembly could be triggered by conditions activating the RhoA-pathway. [12,38] Here we showed that occurrence of solid SFs in the cytoplasm of the MSCs cultured in adherence to plastic surfaces led to a change in indentation of MSCs dependent of their passage and whether MSCs are cultivated in 2D or 3D. For the exact calculation of the Young's modulus, however, it is important to know the extent of indentation, the applied force, and the contact area between the tip and the MSC. To obtain good estimates of the Young's modulus of an individual living MSC, indentation in our experimental system was set to 0.1 µm. With the use of a colloidal AFM cantilever, in addition, the mechanical property of a larger MSC membrane area was measured with high precision. This is of particular importance in P3 adhered MSCs because these cells tend to be the most spread-out cells on the plastic surface but these MSCs showed a surprisingly low Young's modulus of 6.5 ± 6.1 kPa indicating limited disturbance by the plastic surface. Assuming the Young's modulus is not constant over the whole range of indentation, we could segregate an inflection point to further characterize membrane properties. [34,35,37] When the first linear slope E1 was investigated, adherent P1 MSCs showed the steepest incline (ascent: 0.66 ± 0.08), followed by adherent MSCs emerging from aggregates (ascent: 0.41 ± 0.04) and adherent P3 MSCs (ascent: 0.41 ± 0.12). When passing the inflection point, a steep rise of deflection was observed in adherent P1 MSCs (further ascent: 0.97 ± 0.17), while adherent MSCs from aggregates as well as adherent P3 MSCs showed only an additional moderate increase in their curve fit (further ascent: 0.56 ± 0.01). Interestingly, important information could be elaborated from the difference between approach and retraction curve where only adherent MSCs emerging from aggregates had enough driving force to push the AFM tip back to the starting point without any deviation in the retraction curve fit. Adherent P3 MSCs showed the greatest difference between approach and retraction curve most likely due to the negative effect of three rounds of cultivation on MSCs' function.

The migratory capability of MSCs is important for their active contribution to regeneration since MSCs can migrate into injured tissue through peripheral circulation. This trafficking process of MSCs is tightly regulated by a multitude of cytokines, chemokines and bioactive substances, but also biomechanical characteristics of the individual cell including cell size and shape, as well as deformability, membrane and sub-membrane elasticity and to withstand force

from the exterior, can influence this process. Therefore, we have investigated the potential of P1 MSC to close an area of 500 µm in diameter in a commercially available wound closure assay over a period of 24 hours compared the results with P3 MSCs. P3 MSCs were capable to close the gap within 24 h with a migratory dynamic comparable to P1 MSCs when monitored 3, 6 and 12 hours after the onset although their stress fiber and mitochondrial morphology was initially different.

Conclusion

The way of remodeling and fine tuning of the MSC cytoskeleton and mitochondrial network during cultivation is crucial when MSCs are generated for a potential clinical application. Structural adaptation of the actin filaments into dorsal and ventral SFs and the resulting changes in membrane properties can potentially influence MSCs' deformability, shape and migratory capability. Altered mitochondrial morphology with occurrence of mitochondria branches can further influence the balance between growth, differentiation and death of cultured MSCs. When MSCs are applied to provide therapeutic effects, their capability to release their secretome locally at sites of tissue damage or alternatively their potential to integrate and differentiate into multi-lineage specific mature cells relies in part on features taken over by cultivation conditions.

Acknowledgments

The authors thank the company TissueGnostics for technical assistance and the Austrian Cluster for Tissue Regeneration for networking. This work was supported by the Interreg V-A (Nr: ATCZ133) and the N F+B project (Nr: LS15-004).

References

1. Baiguera S, Jungebluth P, Mazzanti B, Mac CP (2012). Mesenchymal stromal cells for tissue-engineered tissue and organ replacements. Transplant International 25(4): 369-382.
2. Girolamo L, Sartori MF, Arrigoni E, Rimondini L, Albisetti W, et.al. (2008) Human adipose-derived stem cells as future tools in tissue regeneration: Osteogenic differentiation and cell-scaffold interaction. Int. J. Artif. Organs 31(6); 467-479.
3. Burridge K, Erika SW (2013) The tension mounts: Stress fibers as force-generating mechanotransducers. J. Cell Biol 200(1): 9-19.
4. Yourek G, Hussain MA, Mao JJ (2007) Cytoskeletal changes of mesenchymal stem cells during differentiation. ASAIO J 53(2):219-228.
5. Harris G, Piroli M, Jabbarzadeh E (2014) Deconstructing the Effects of Matrix Elasticity and Geometry in Mesenchymal Stem Cell Lineage Commitment. Adv funct Mater 24(16): 2396-2403.
6. Gattazzo F, Urciuolo A, Bonaldo P (2014) Extracellular matrix: A dynamic microenvironment for stem cell niche. Biochim. Biophys. Acta-Gen 1840(8): 2506-2519.
7. Chun Y, Frank WD, Hao M, Anouk RK, Lena PB, et.al. (2016) Spatially patterned matrix elasticity directs stem cell fate. Proc Natl Acad Sci 113(31): 4439-4445.
8. Sharona E, Vira A, Kenneth MY (2006) Matrix Control of Stem Cell Fate Cell. 126(4): 645-647.
9. Santis SD, Lennon AB, Boschetti F, Verhegghe B, Verdonck P,et.al. (2011) How can cells sense the elasticity of a substrate? an analysis using a cell tensegrity model. Eur Cells Mater 22:202-213.
10. Dominici M, Blanc KL, Mueller I, Slaper C, Marini Fc, et.al. (2006) Minimal criteria for defining multipotent mesenchymal stromal cells. The International Society for Cellular Therapy position statement', Cytotherapy 8(4): 315-331.
11. Squillaro T, Peluso G, Galderisi U (2016) Clinical Trials With Mesenchymal Stem Cells: An Update. Cell Transplant 25(5):829-848.
12. Burridge K, Guilluy C (2016) Focal adhesions, stress fibers and mechanical tension', Exp. Cell Res 343(1):14-20.
13. Atherton P, Stutchbury B, Jethwa D, Ballestrem C (2016) Mechanosensitive components of integrin adhesions: Role of vinculin. Exp Cell Res 343(1): 21-27.
14. Bays JL, Peng X, Tolbert CE, Guilluy C, Angell A, et.al. (2014). Vinculin phosphorylation differentially regulates mechanotransduction at cell–cell and cell–matrix adhesions. J Cell Bio 205(2): 251-263.
15. Andrew WH, Xinyi T, Deepthi V, Ludovic GV, Alexander F, et.al. (2013) In situ mechanotransduction via vinculin regulates stem cell differentiation. Stem Cells 31(11):2467-77.
16. Mullen CA, Vaughan TJ, Voisin MC, Brennan MA, Layrolle P (2014) Cell morphology and focal adhesion location alters internal cell stress. J. R. Soc. Interface 11(101): 20140885–20140885.
17. Mark AS, Elizabeth B, Margaret LG, Laura L, Clare MW, et.al. (2010) A zyxin-mediated mechanism for actin stress fiber maintenance and repair. Dev Cell 19(3):365-376.
18. Adam SZ,Felicia CL,Ran L,Michael R ,Krystyn JV, et.al. (2012) Macromolecular crowding directs extracellular matrix organization and mesenchymal stem cell behavior. PLoS One 7(5):37904.
19. Lynch K, Pei M (2014) Age associated communication between cells and matrix: a potential impact on stem cell-based tissue regeneration strategies. Organogenesis 10(3): 289-298.
20. Zhou Y, Chen H, Li H, Wu Y (2017) 3D culture increases pluripotent gene expression in mesenchymal stem cells through relaxation of cytoskeleton tension. J Cell Mol Med 21(6):` 1073-1084.
21. Hosseini MS, Tafazzoli-Shadpour M, Haghighipour N, Aghdami N, Goodarzi A, et.al. (2015) 'The synergistic effects of shear stress and cyclic hydrostatic pressure modulate chondrogenic induction of human mesenchymal stem cells. Int J Artif Organs 38(10):557-564.
22. Walters B (2017) Engineering the geometrical shape of mesenchymal stromal cells through defined cyclic stretch regimens. Sci Rep 7(1):6640.
23. Niepel MS, Almouhanna F, Ekambaram BK, Menzel M, Heilmann A, et.al. (2018) Cross-linking multilayers of poly-l-lysine and hyaluronic acid: Effect on mesenchymal stem cell behavior. Int J Artif Organs 41(4).
24. Hsu YC, Wu YT, Yu TH, (2016) Mitochondria in mesenchymal stem cell biology and cell therapy: From cellular differentiation to mitochondrial transfer. Semin Cell Dev Biol 52:119-131.
25. Zemirli N, Morel E, Molino D (2018) Mitochondrial dynamics in basal and stressful conditions', International Journal of Molecular Sciences. 19(2), 564.
26. Seung MY, Yong KJ (2018) A Molecular Approach to Mitophagy and Mitochondrial Dynamics. Mol Cells 41(1):18-26.
27. Soncini M (2007) Isolation and characterization of mesenchymal cells from human fetal membranes. J Tissue Eng Regen Med 1(4): 296-305.
28. Walzer SM (2019) A 3-Dimensional In Vitro Model of Zonally Organized Extracellular Matrix. Cartilage 1-10.
29. Butt HJ, Jaschke M (1995) Calculation of thermal noise in atomic force microscopy. Nanotechnology 6(1).
30. Hertz H (1882) About the touch of solid elastic bodies. J Pure and Applied Math 92:156-171.
31. Sneddon IN (1965) The relation between load and penetration in the axisymmetric bossiness problem for a punch of arbitrary profile. Int J Eng Sci 3(1) 47-57.
32. Rychtárikova R, Stys D (2017) Observation of dynamics inside an unlabeled live cell using a bright-field photon microscopy: Evaluation of organelles trajectories.
33. Rychtárikova R, Korbel J, Macháček P, Stys D, (2018) Point Divergence Gain and Multidimensional Data Sequences Analysis. Entropy.
34. Carl P, Schillers H (2008) Elasticity measurement of living cells with an atomic force microscope: Data acquisition and processing. Pflugers Arch Eur J Physiol 457(551).
35. Zhao Y, Zhang TB, Bao CH, Chen H, Wang Y (2013) Physical properties of gastrointestinal stromal tumors based on atomic force microscope analysis. Genet Mol Res 12, 5774-5785.
36. Abstracts from the 45th ESAO Congress 12–15 September 2018, Madrid, Spain (2018) Int J Artif Organs 41(9): 486-631.

37. Melzak KA, Toca-Herrera JL (2015) Atomic force microscopy and cells: Indentation profiles around the AFM tip, cell shape changes, and other examples of experimental factors affecting modeling. Microsc Res Tech 78(7): 626-632.

38. Ridley AJ, Hall A (1992) The small GTP-binding protein rho regulates the assembly of focal adhesions and actin stress fibers in response to growth factors. Cell 70(3):389-99.

Author Affiliations

Top

[1]*Department for Biomedical Research, Center for Experimental Medicine, Danube University Krems, Austria*

[2]*Institute of Complex Systems, Faculty of Fisheries and Protection of Waters, University of South Bohemia in České Budějovice, Nove Hrady, Czech Republic*

[3]*Clinic for Orthopedic Surgery, Karl Chiari Research Laboratories, Austria*

[4]*Core Facility Imaging, Medical University Vienna, Vienna, Austria*

[5]*Christian Doppler Laboratory for Innovative Therapy Approaches in Sepsis, Danube University Krems, Krems, Austria*

[6]*Clinic for Blood Group Serology and Transfusion Medicine, University Krems, Krems, Austria*